Article

Chinese Science Bulletin

Geology

June 2012 Vol.57 No.18: 2289–2301
doi: 10.1007/s11434-012-5069-3

Petrogenesis of Aoyougou high-silica adakite in the North Qilian orogen, NW China: Evidence for decompression melting of oceanic slab

CHEN YuXiao, XIA XiaoHong & SONG ShuGuang*

MOE Key Laboratory of Orogenic Belts and Crustal Evolution, School of Earth and Space Sciences, Peking University, Beijing 100871, China

Received January 6, 2012; accepted February 14, 2012; published online April 24, 2012

A trondhjemitic body occurs in the Aoyougou area, the western part of the North Qilian orogen. It is geochemically characterized by high SiO_2, Na_2O (high Na/K), elevated Sr/Y and $(La/Yb)_N$, positive Sr anomaly, relatively enriched large ion lithophile elements (LILEs) and light rare earth elements (LREEs), and depleted Nb, Ta, Ti, resembling the high-silica adakite. Zircon U-Pb SHRIMP dating yields a weighted mean age of 438±3 Ma. This age is significantly younger than eclogitization ages of 460–490 Ma in the North Qilian orogen, suggesting that formation of the adakite postdates the subduction of oceanic crust in association with closure of the ancient Qilian Ocean. Whole-rock Sr and Nd isotopic analyses give initial ratios of I_{Sr}=0.7044–0.7047 and $\varepsilon_{Nd}(t)$=3.0–4.1, indicating that they are derived from partial melting of the juvenile oceanic crust. In view of the tectonic evolution of the North Qilian orogen, the high-silica adakite was probably derived from decompression melting of the exhumed eclogite at the depth of ~60 km.

high-silica adakite, Early Silurian, eclogite, melting during exhumation, west segment of the North Qilian Mountain

Citation: Chen Y X, Xia X H, Song S G. Petrogenesis of Aoyougou high-silica adakite in the North Qilian orogen, NW China: Evidence for decompression melting of oceanic slab. Chin Sci Bull, 2012, 57: 2289–2301, doi: 10.1007/s11434-012-5069-3

The terminology "adakite" is referred to a series of igneous rocks that are characterized by low Y, elevated Sr, Sr/Y and $(La/Yb)_N$ [1]. The petrogenesis of adakite is of great significance and has been hotly discussed, not only for the tectonic reconstruction of the ancient ocean and plate [1–6], but also for the origin of the continent crust dominated by Archaean tonalite-trondhjemite-granodiorite (TTG) [7–12].

Adakite is originally linked to melting of young and hot slab, and mainly distributes in the circum-Pacific margins [7,8,13,14]. However, recent studies have revealed that partial melting of thickened lower crust and differentiation of parental basaltic magma at high pressure are also possible mechanisms [15–25]. This implies that adakite is of diverse derivation and the slab melting model, to some extent, has defect as extremely limited conditions for melting, thus prerequisites such as high geothermal gradient, relatively hot and juvenile slab, flat subduction and slab window have been proposed [1,6,7,26]. Heat source plays a key role in the formation of magma, but absolutely not the unique one [27]. Decompression melting has been confirmed to be one of the most important mechanisms for magma generation. For instance, it is common that when metamorphic rocks exhume to the Earth's surface, break-down of hydrous minerals will decrease the solidus line of surrounding rocks, inducing melting due to pressure-decreasing [28–32].

This paper presents geochemical, Sr-Nd isotopic and geochronological data for an Early Silurian-aged high-silica adakite in the west segment of the North Qilian orogen. Combining the temporal relation with formation of eclogite and tectonics of the North Qilian Orogen, we suggest that the adakitic magma is generated by decompression melting of eclogite during exhumation. This model provides a new explanation for the origin of adakite, as well as tectonic evolution of the North Qilian orogen in Early Paleozoic time.

*Corresponding author (email: sgsong@pku.edu.cn)

1 Geological background

The North Qilian orogenic belt in the northern Qinghai-Tibet Plateau is a well-studied Early Paleozoic suture zone in China. It extends in the NW direction between the Alashan block to the north and the Qaidam block to the south, and is offset by the Altyn Tagh fault, a largest sinistral-slip fault in NW China, to the west [33]. This suture zone consists predominantly of subduction accretionary complexes, including ophiolite, high-pressure metamorphic rocks, arc volcanic rocks, granitic intrusives, Silurian flysch formation, Devonian molasses and post-Devonian sedimentary covers [34,35] (Figure 1a).

The Aoyougou trondhjemitic pluton is located in the

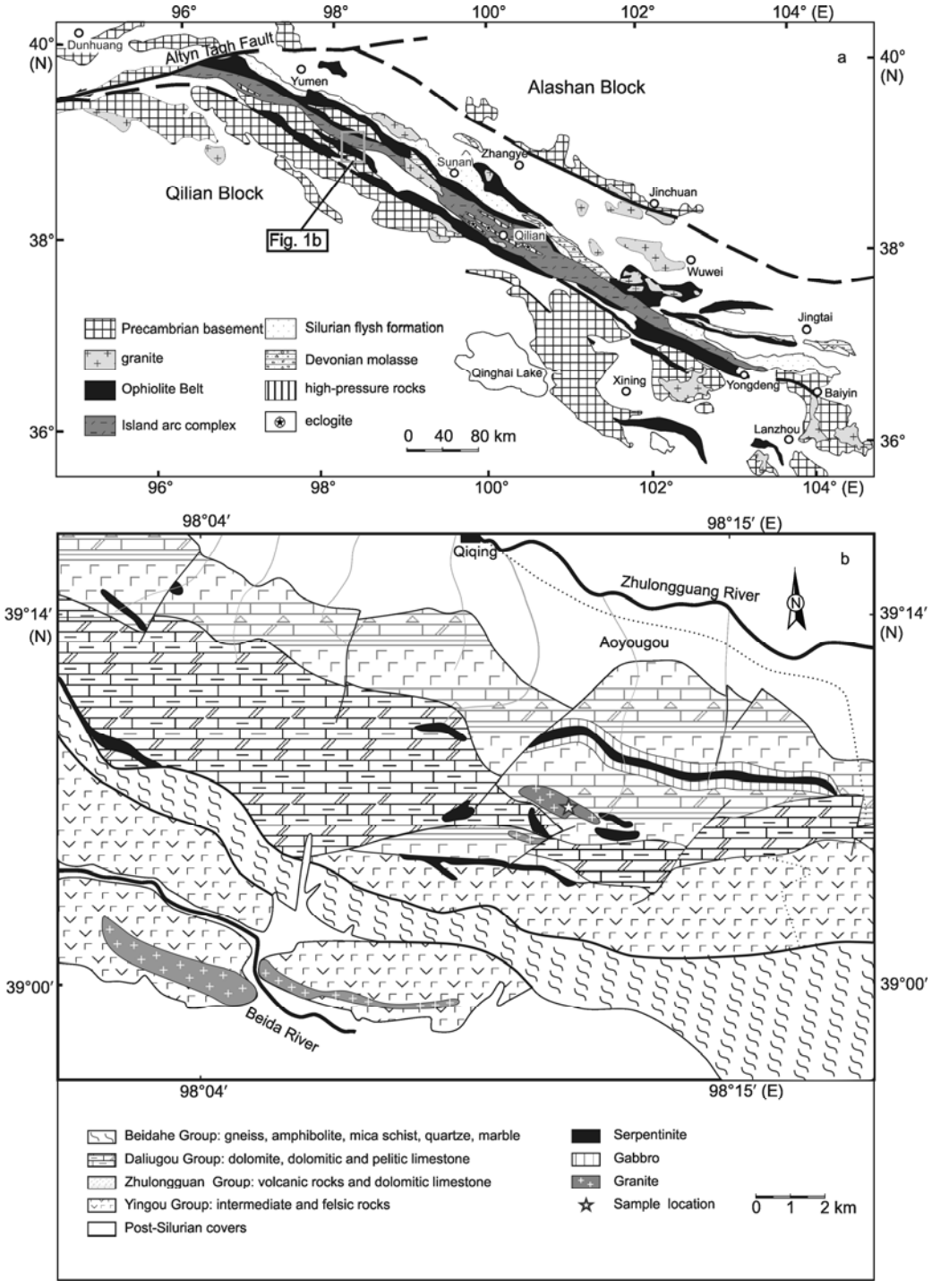

Figure 1 a, Schematic geological map of the North Qilian orogenic belt (after [38]); b, geological map of Aoyougou region (modified after 1: 200000 Qilianshan map).

western segment of the North Qilian orogen. It lies approximately 8 km to the southeast of Qiqing town, Sunan County, Gansu Province. To the north is the famous Aoyougou ophiolite that comprises of serpentinized peridotite, gabbro and basalt [36]. Zircons from gabbro gave an age of 504±6 Ma by SHRIMP U-Pb dating [37]. The trondhjemitic pluton is an ovoid body of ~1 km^2 in size (Figure 1b) and intrudes in mafic volcanic rocks of the Zhulongguan group (Figure 2a) with a chilling margin. Country rocks near the boundary are remarkably baked (Figure 2b).

2 Petrography

The Aoyougou trondhjemite consists of plagioclase (60%–70%), quartz (~20%), K-feldspar (<5%), mafic minerals (<5%, mostly chloritized) and minor accessory minerals such as apatite, zircon, titanite and exhibits typical coarse-grained granitic texture. Plagioclase grains are euhedral and slightly saussuritized and sericitized. Some grains show clear magmatic oscillatory zoning (Figure 2d) with An values decreasing from core (33.56) to rim (10.75) (Table 1), reflecting crystal fractionation of the adakitic magma.

3 Zircon U-Pb geochronology

Sample 09AY-14 was chosen for dating and zircon separation was done in a laboratory of Langfang Institute of Regional Geological Survey. Zircon grains were separated with the assistance of standard heavy liquid and magnetic techniques and then hand-picked under a binocular microscope. They were mounted in a 25 mm epoxy disc together with zircon standard M257 and TEMORA and polished to half-sections. The internal structure of zircon grains were examined by cathodoluminescent (CL) image using a FEI PHILIPS XL30 SFEG Scanning Electron Microscope (SEM) with 2-min scanning time in condition 15 kV/120 nA in School of Physics, Peking University. The zircon grains were analyzed for U-Th-Pb isotopes using the sensitive high-resolution ion microprobes (SHRIMP II) at Curtin University of Technology, Western Australia. The instrument was controlled and data acquired from a remote control centre in the Beijing SHRIMP Centre, Institute of Geology, CAGS, Beijing. This was achieved via the SHRIMP Remote Operation System (SROS) which allows the remote operator to control the instrument, choose sites for analysis and data print out in real time through internet. Zircon Standard

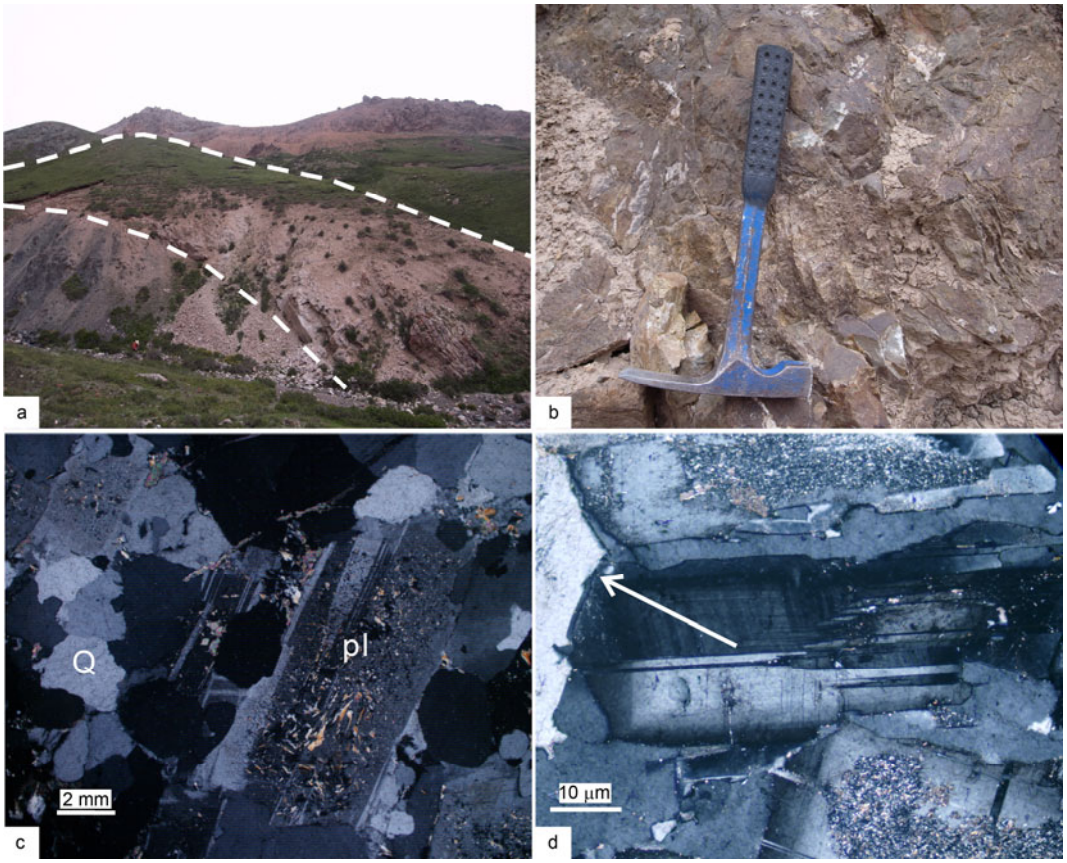

Figure 2 Field and photomicrographs of the Aoyougou trondhjemite. a, Trondhjemitic body intruding in mafic rocks of the Zhulongguan Group; b, the fine-grained chilling margin near the contact boundary; c, medium- to coarse-grained granitic texture (10QL-16); d, plagioclase showing magmatic crystallization zoning (10QL-18).

Table 1 Chemical analyses of a plagioclase grain from the Aoyougou trondhjemite (10QL-18) from core (3.1) to rim (3.13)

No.	3.1	3.2	3.3	3.4	3.5	3.6	3.7	3.8	3.9	3.10	3.11	3.12	3.13
SiO_2	59.36	59.39	59.88	59.72	59.99	59.53	60.02	59.64	61.23	61.98	61.97	63.78	65.76
TiO_2	0.00	0.04	0.02	0.01	0.00	0.04	0.00	0.04	0.00	0.04	0.00	0.03	0.00
Al_2O_3	24.82	25.51	25.69	25.81	25.70	26.21	25.52	25.58	24.81	24.27	23.90	22.67	21.87
Cr_2O_3	0.00	0.00	0.00	0.03	0.02	0.00	0.02	0.00	0.00	0.02	0.00	0.08	0.00
FeO	0.22	0.11	0.15	0.13	0.18	0.19	0.17	0.13	0.04	0.08	0.13	0.10	0.02
MnO	0.03	0.00	0.00	0.00	0.00	0.06	0.02	0.00	0.03	0.00	0.04	0.02	0.01
MgO	0.01	0.02	0.00	0.03	0.00	0.05	0.01	0.03	0.02	0.01	0.00	0.00	0.00
CaO	6.40	7.19	7.06	6.90	6.88	7.10	6.62	6.90	5.89	5.58	4.81	3.88	2.28
Na_2O	8.03	7.76	8.01	7.77	7.94	7.58	8.14	8.26	8.30	8.49	8.96	9.49	10.34
K_2O	0.25	0.14	0.17	0.18	0.18	0.13	0.12	0.16	0.18	0.18	0.25	0.35	0.19
NiO	0.00	0.09	0.00	0.00	0.00	0.02	0.05	0.01	0.04	0.05	0.00	0.00	0.00
Total	99.12	100.25	100.98	100.58	100.90	100.91	100.68	100.75	100.55	100.69	100.06	100.39	100.47
An	30.18	33.56	32.46	32.60	32.06	33.84	30.75	31.30	27.87	26.40	22.61	18.05	10.75
Ab	68.46	65.66	66.57	66.40	66.96	65.46	68.56	67.84	71.13	72.60	76.01	79.98	88.14
Or	1.37	0.78	0.97	0.99	0.98	0.70	0.69	0.86	1.00	1.00	1.38	1.97	1.11

M257 ($^{206}Pb/^{238}U$ expected age: 572 Ma, U concentration: 238 ppm) was measured to calibrate U, Th and Pb concentrations, and standard zircon TEM ($^{206}Pb/^{238}U$ expected age: 417 Ma) was used for element fractionation correction. Data reduction was conducted by SQUID1.0 software, and Concordia diagrams of age data were generated using ISOPLOT program [39]. Uncertainties in ages are given at the 1σ level. Final weighted mean ages are quoted with 95% (2σ) confidence limits. The detailed analytical procedures and principium were described in references [40,41]. Results are presented in Table 2.

Zircon grains from 09AY-14 are colorless, euhedral crystals in size of 150–120 μm long and 20–40 μm wide and show clear concentric oscillatory zoning in CL images (Figure 3). Thirteen representative zircons are chosen for U-Th-Pb analysis; U and Th contents in zircons are relatively low, ranging from 99 to 162 ppm for U and from 46 to 97 ppm for Th with Th/U ratios of 0.46–0.65 (Table 2). All analyzed spots give a limited range of $^{206}Pb/^{238}U$ ages from 431 to 441 Ma with a weighted mean of 438±3 Ma (MSWD= 0.46) (Figure 4). Thus, the age of 438±3 Ma can represent the forming age of the Aoyougou trondhjemite.

Table 2 SHRIMP U-Th-Pb analyses for zircons from the Aoyougou trondhjemite[a)]

No.	U (ppm)	Th (ppm)	Th/U	$^{206}Pb^*$ (ppm)	$^{206}Pb_c$/%	$^{207}Pb^*/^{235}U$	±%	$^{206}Pb^*/^{238}U$	±%	$^{206}Pb/^{238}U$ Age (Ma)	±1
1	104	51	0.51	6.15	0.00	0.5202	3.4	0.0691	1.4	431.0	6.0
2	104	53	0.52	6.23	0.00	0.5380	3.4	0.0695	1.4	433.1	6.0
3	99	46	0.48	5.98	0.19	0.5291	4.1	0.0700	1.5	436.4	6.3
4	122	60	0.51	7.42	0.00	0.5671	3.3	0.0709	1.4	441.6	6.0
5	113	57	0.52	6.95	0.37	0.5233	4.5	0.0713	1.5	444.2	6.3
6	162	76	0.48	9.87	0.68	0.5538	5.3	0.0705	1.3	438.9	5.6
7	129	57	0.46	7.88	0.00	0.5188	3.2	0.0709	1.4	441.8	5.9
8	157	86	0.57	9.52	0.16	0.5012	3.1	0.0706	1.3	439.5	5.5
9	103	50	0.50	6.17	0.00	0.5340	3.4	0.0699	1.4	435.4	6.0
10	157	97	0.64	9.37	0.11	0.5218	3.4	0.0694	1.9	432.3	7.8
11	128	70	0.56	7.82	0.18	0.5064	3.3	0.0708	1.3	441.0	5.7
12	150	94	0.65	9.02	0.00	0.5285	2.8	0.0699	1.3	435.4	5.4
13	124	66	0.55	7.53	0.23	0.5224	3.5	0.0708	1.4	441.2	5.8

a) $^{206}Pb_c$ and $^{206}Pb^*$, Common and radiogenic portions. Common Pb was corrected using measured ^{204}Pb.

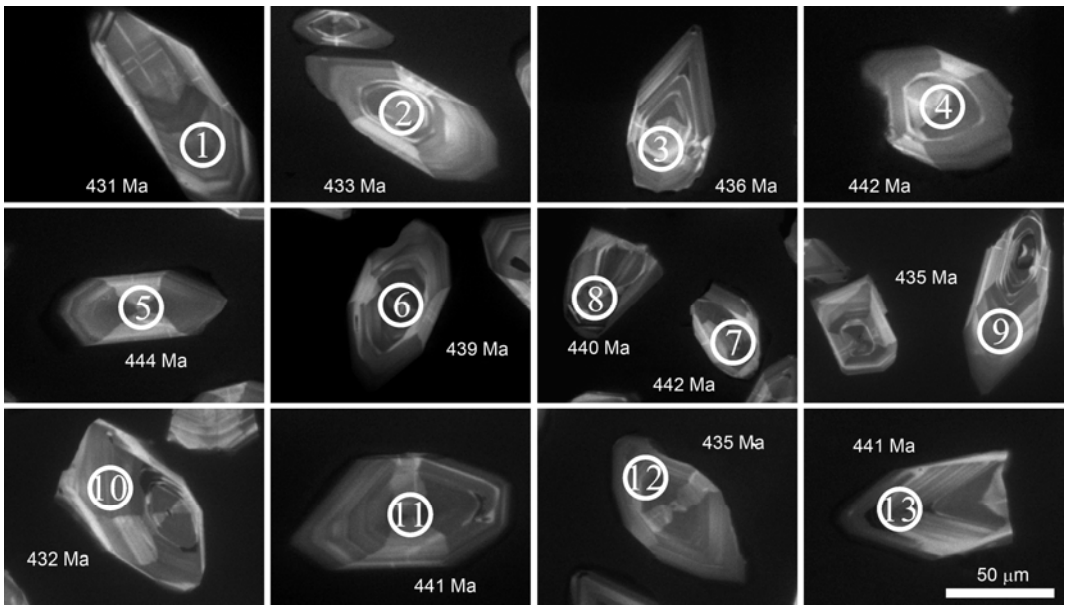

Figure 3 CL images for zircons and analytic spots with ages.

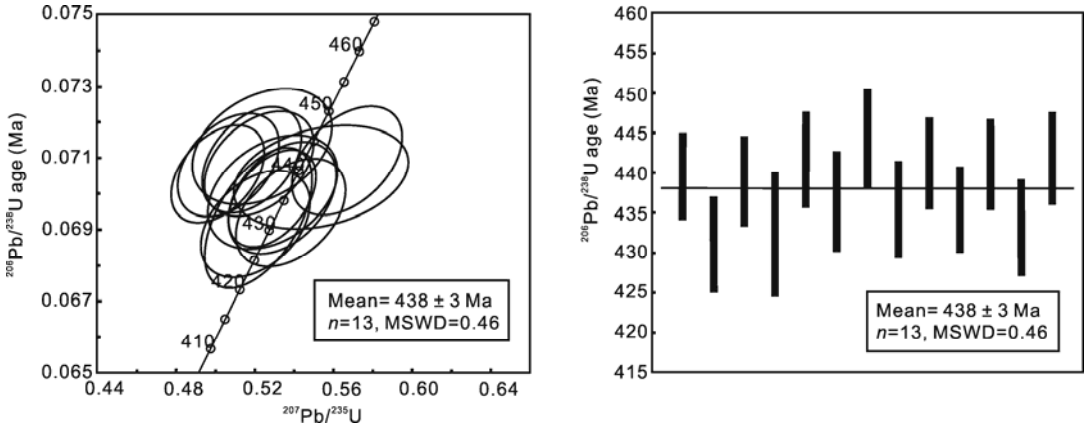

Figure 4 Concordia and average diagrams for zircons from the Aoyougou trondhjemite.

4 Geochemistry

4.1 Analytical methods

The whole-rock major and trace elements were determined by Leeman Prodigy inductively coupled plasma-optical emission spectroscopy (ICP-OES) and Agilent-7500a inductively coupled plasma mass spectrometry (ICP-MS) at China University of Geosciences, Beijing, respectively. Precisions (1δ) for almost all elements are less than 1%, except for TiO_2 (~1.5%) and P_2O_5 (~2.0%). Loss on igition (LOI) was performed by placing 1g of samples in the furnace keeping 1000°C for several hours and being reweighed after cooled. More details should be related to [42]. Results are listed in Table 3.

100–150 mg powders of three fresh samples (09AY-14, 17 and 10QL-15) and BCR-2 standard were dissolved using $HClO_4$ and HF in Teflon vessels and Sr and Nd elements were achieved by further separation work in Peking University, Beijing. The analyses were performed on a Triton T1 Mass Spectrometry in the Institute of Geology and Mineral resources, Tianjin. Detail procedure follows that of Jahn et al [43]. During the course of this study, the mean $^{87}Sr/^{86}Sr$ ratios for NBS-987 and BCR-2 are 0.710238±5 (n=3) and 0.705016±3 (n=2), respectively, while the mean $^{143}Nd/^{144}Nd$ ratio was 0.512118±6 (n=5) for JNDI and 0.512637±6 (n=2) for BCR-2. Results are shown in Table 4.

4.2 Results

All the nine samples in Table 3 are characterized by high contents of SiO_2 (67.3 wt.%–74.1 wt.%), Na_2O (4.76 wt.%–9.05 wt.%), and extremely low K_2O/Na_2O ratios (0.12–0.34). In the K-Na-Ca triangle (Figure 5), all samples plot in the Archean TTG field and display along the evolutionary trend of trondhjemitic magma. In the K_2O-SiO_2 diagram (Figure 6a),

Table 3 Whole-rock major (wt.%) and trace element (ppm) compositions of Aoyougou trondhjemites

Sample	09AY14	09AY15	09AY16	09AY17	10QL15	10QL16	10QL20	10QL21	10QL23
SiO_2	72.41	70.96	70.52	69.53	74.07	73.63	72.83	67.26	71.64
TiO_2	0.15	0.16	0.17	0.17	0.16	0.15	0.16	0.18	0.16
Al_2O_3	14.98	14.87	15.39	16.51	14.52	14.58	15.17	18.37	15.25
Fe_2O_3	0.69	0.77	0.92	0.74	1.15	1.05	1.13	1.34	1.06
MnO	0.02	0.02	0.02	0.01	0.01	0.01	0.02	0.02	0.02
MgO	0.66	0.74	0.82	0.69	0.70	0.66	0.77	0.83	0.55
CaO	2.23	2.07	1.36	0.83	1.33	1.70	1.41	2.90	2.43
Na_2O	6.04	6.76	7.89	9.05	5.02	4.76	5.32	5.75	4.77
K_2O	1.59	1.43	1.12	1.04	1.47	1.38	1.27	1.70	1.62
P_2O_5	0.05	0.06	0.06	0.06	0.05	0.05	0.06	0.06	0.05
LOI	1.06	2.03	1.62	1.29	0.86	1.40	1.18	0.75	1.75
Total	99.87	99.86	99.89	99.94	99.35	99.35	99.32	99.17	99.31
K_2O/Na_2O	0.26	0.21	0.14	0.12	0.29	0.29	0.24	0.30	0.34
Li	2.27	2.13	3.95	2.22	0.39	0.55	0.74	8.30	0.42
Sc	2.25	2.21	2.09	2.32	2.03	1.89	2.15	2.24	2.01
V	15.40	16.33	16.22	15.77	16.81	16.03	16.80	17.62	15.59
Cr	8.55	9.52	9.97	10.40	22.43	11.17	13.00	11.13	9.19
Co	3.01	2.68	3.30	2.26	3.26	2.56	3.17	3.41	2.08
Ni	6.17	6.20	6.88	6.38	12.89	6.90	8.02	7.36	7.41
Cu	2.21	2.62	2.65	3.55	4.35	1.62	1.23	1.31	0.97
Zn	94.65	32.68	40.42	31.02	28.42	22.38	26.84	36.88	23.26
Ga	15.39	15.36	14.81	13.91	16.30	16.06	16.84	18.07	16.40
Rb	28.18	33.32	25.02	25.60	33.66	36.94	35.65	40.70	42.06
Sr	661	739	539	212	782	551	521	764	552
Y	2.96	2.64	2.58	2.96	3.00	2.62	2.80	3.41	2.96
Zr	80.5	75.6	91.1	78.8	108.7	88.9	97.3	122.5	89.7
Nb	1.18	1.26	1.22	1.46	1.77	1.67	1.98	1.94	1.97
Cs	0.18	0.33	0.33	0.21	0.22	0.46	0.58	0.69	0.47
Ba	433	408	334	183	986	464	363	580	475
La	4.83	4.19	4.90	4.68	8.08	5.66	5.80	6.48	4.84
Ce	10.36	9.34	10.55	10.33	15.97	11.62	12.04	13.42	10.15
Pr	1.25	1.14	1.27	1.23	1.91	1.42	1.48	1.65	1.27
Nd	4.85	4.54	4.95	4.78	7.56	5.68	5.98	6.70	5.21
Sm	0.99	1.00	1.00	1.00	1.33	1.01	1.09	1.22	0.99
Eu	0.30	0.30	0.31	0.20	0.35	0.22	0.25	0.31	0.25
Gd	0.87	0.83	0.81	0.84	1.03	0.79	0.85	0.99	0.85
Tb	0.11	0.10	0.10	0.11	0.12	0.10	0.11	0.12	0.11
Dy	0.52	0.49	0.47	0.57	0.60	0.51	0.54	0.64	0.57
Ho	0.09	0.08	0.09	0.10	0.10	0.09	0.10	0.11	0.10
Er	0.24	0.21	0.21	0.25	0.24	0.22	0.23	0.28	0.24
Tm	0.04	0.03	0.03	0.03	0.03	0.03	0.03	0.04	0.03
Yb	0.21	0.18	0.19	0.22	0.21	0.20	0.22	0.26	0.21
Lu	0.03	0.03	0.03	0.03	0.03	0.03	0.03	0.04	0.03
Hf	1.90	1.71	2.09	1.87	2.61	2.14	2.38	2.85	2.23
Ta	0.08	0.07	0.08	0.09	0.13	0.12	0.13	0.13	0.17
Pb	6.27	5.23	6.48	6.89	8.47	6.99	6.01	10.43	8.54
Th	0.96	0.92	0.98	0.99	2.16	0.88	0.92	1.06	0.91
U	0.43	0.36	0.42	0.51	0.61	0.45	0.49	0.55	0.48
Sr/Y	223	280	209	72	261	210	186	224	187
$(La/Yb)_N$	16.60	16.30	18.88	14.99	27.79	20.35	19.19	17.94	16.29

Table 4 Sr and Nd isotopic data of Aoyougou trondhjemites[a)]

Sample	$^{87}Rb/^{86}Sr$	$^{87}Sr/^{86}Sr$	2σ	$I_{Sr}(t)$	$^{147}Sm/^{144}Nd$	$^{143}Nd/^{144}Nd$	2σ	t(Ma)	$\varepsilon_{Nd}(0)$	$\varepsilon_{Nd}(t)$	$f_{Sm/Nd}$	T_{DM2}
09AY-14	0.124	0.7054	3	0.7047	0.124	0.5126	12	438	0.05	4.1	–0.37	836
10QL-15	0.125	0.7052	4	0.7044	0.106	0.5126	5	438	–1.25	3.8	–0.46	869
09AY-17	0.350	0.7069	7	0.7047	0.127	0.5126	7	438	–0.96	3.0	–0.36	932

a) $^{143}Nd/^{144}Nd_{CHUR}=0.512638$, $^{147}Sm/^{144}Nd_{CHUR}=0.1967$, $^{143}Nd/^{144}Nd_{DM}=0.51315$, $^{147}Sm/^{144}Nd_{DM}=0.2135$; $\lambda_{Rb}=1.42\times10^{-11}$/a, $\lambda_{Sm}=6.54\times10^{-12}$/a. The two-stage model ages were calculated according to [46].

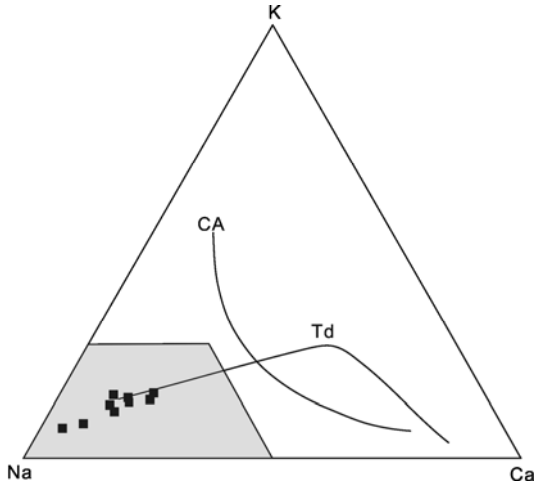

Figure 5 K-Na-Ca triangle [44]. CA, Classical calc-alkaline trend; Td, trondhjemitic differentiation trend; grey field: Archean TTG [45].

all samples project between the low-K tholeiitic and calc-alkaline series within the high-silica adakite (HSA) field of modern subduction zones, much different from adakitic rocks in the North China Craton.

Compared with the low-silica adakite (LSA) and high-silica adakite (HSA) subdivided by Martin et al. [8], eight of the nine samples share distinct similarity with HSA (Figure 6a–h). They are characterized by enriched LREE and depleted HREE with Yb (0.18–0.26 ppm) and $(La/Yb)_N$ (16.3–27.8), elevated Sr (521–782 ppm), depressed Y (2.58–3.41 ppm), and high Sr/Y ratios (186–280), analogous to those features of adakite. The primitive mantle-normalized spider diagram displays positive Pb, Sr, Zr and Hf anomaly and negative Nb, Ta and Ti anomaly (Figure 7a). The chondrite-normalized REE pattern exhibits a steep right-slant pattern (Figure 7b). In the Sr/Y-Y and $(La/Yb)_N$-Yb_N discrimination diagrams, all samples from the Aoyougou trondhjemite resemble the typical adakite, but distinct from classical island-arc calc-alkaline magma (Figure 8). Sample 09AY-17 exhibits lower CaO, Sr (212 ppm), Sr/Y ratio (72) than other samples and shows weakly negative Eu anomaly, which can be interpreted as fractional crystallization of plagioclase when melt rises.

The present-day $^{87}Sr/^{86}Sr$ and $^{143}Nd/^{144}Nd$ ratios from three samples (09AY-14, 17 and 10QL-15) in this study are 0.7054–0.7069 and 0.5126–0.5126, respectively. Considering the emplacement age of this trondhjemitic melt and the measured Rb/Sr and Sm/Nd ratios, the initial Sr ratios (I_{Sr}), ε_{Nd} (t) values and the two-stage Nd model ages (T_{DM2}) vary in the range of 0.7044–0.7047, 3.0–4.1 and 836–932 Ma, respectively.

5 Discussion

Zircon ages of eclogites in the North Qilian suture zone range from 460 to 490 Ma [33,48,49], and Ar-Ar dating ages of glaucophane and phengite in blueschists are from 440 to 460 Ma [50–52]. The closure of the ancient Qilian Ocean is believed to be in Late Ordovician (approximately 445 Ma) through integration of abundant information such as arc-related magma, Silurian flysch formation and Devonian molasses [33,35,53,54]. Zircons from the Aoyougou trondhjemite yield an age of 438±3 Ma; this age is later than either eclogites or blueschists, but approaches to the closure time of Qilian Ocean. Based on these observations, origin of the Aoyougou trondhjemite is mostly associated with closure of the Qilian Ocean and subsequent continent collision.

Experiments demonstrate that the adakitic melt can be generated by partial melting of meta-basalts under the pressure (>1.0 GPa) where garnet remains stable [55–57]. On the basis of rock types and forming mechanisms, it is generally thought that adakite can be achieved by three ways: (1) partial melting of subducted slab [1–6,14], (2) partial melting of thickened lower crust [15–21,25], and (3) high-pressure fractional crystallization of basaltic magma [22,24]. The Aoyougou trondhjemitic rocks have I_{Sr} of 0.7044–0.7047 and ε_{Nd} (t) of 3.0–4.1, suggesting that they are originated from a juvenile oceanic crust rather than the old continental lower crust.

All samples in this study are sodic with K_2O/Na_2O ranging from 0.12 to 0.34, much lower than those from lower continental crust (nearly 0.5). Moreover, the Sr and Nd isotopic data of our samples are in contrast with those of lower crust origin (e.g. Adakites in Tibet, North Qilian and Cordillera Blanca Batholith) (Figure 9). Although these samples exhibit somewhat higher I_{Sr} and lower $\varepsilon_{Nd}(t)$ values than some modern adakites considered as slab melting, it should be noted that, thanks to source contamination in subduction zones, adakites (e.g. adakites in Austral Volcanic Zone and Tonga [14,58]) and eclogites (e.g. eclogites from the North Qaidam (Figure 9) and Alpine (2.3–7.8) [59,60]) have similar

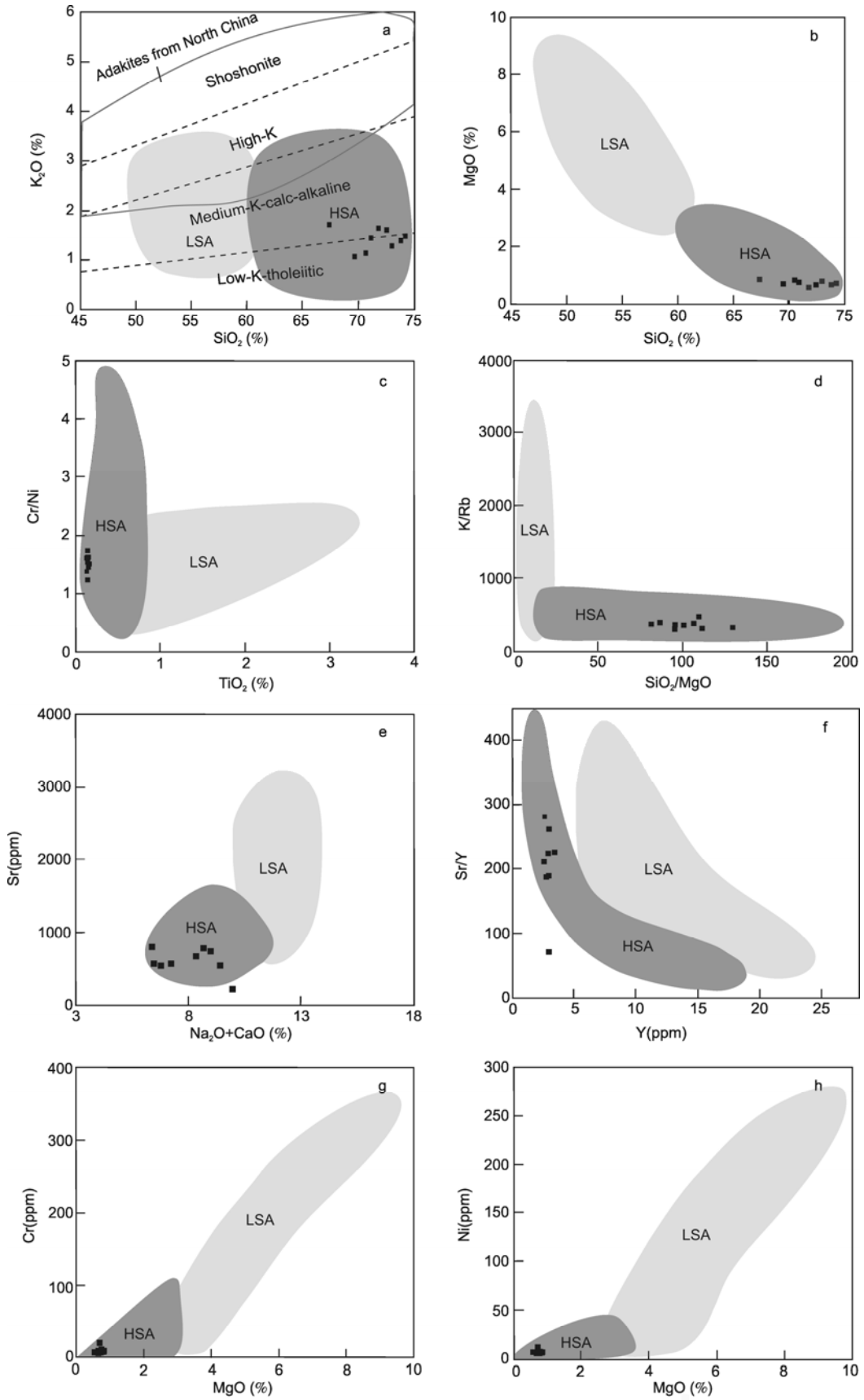

Figure 6 Diagrams of K_2O vs. SiO_2 (a), MgO vs. SiO_2 (b), (Cr/Ni) vs. TiO_2 (c), (K/Rb) vs. (SiO_2/MgO) (d), Sr vs. (Na_2O+CaO) (e), (Sr/Y) vs. Y(f), Cr vs. MgO (g), and Ni vs. MgO (h). Light grey field: low sillica adakite (LSA); dark grey field: high sillica adakite (HSA) [8]; solid line: adakite from North China [21].

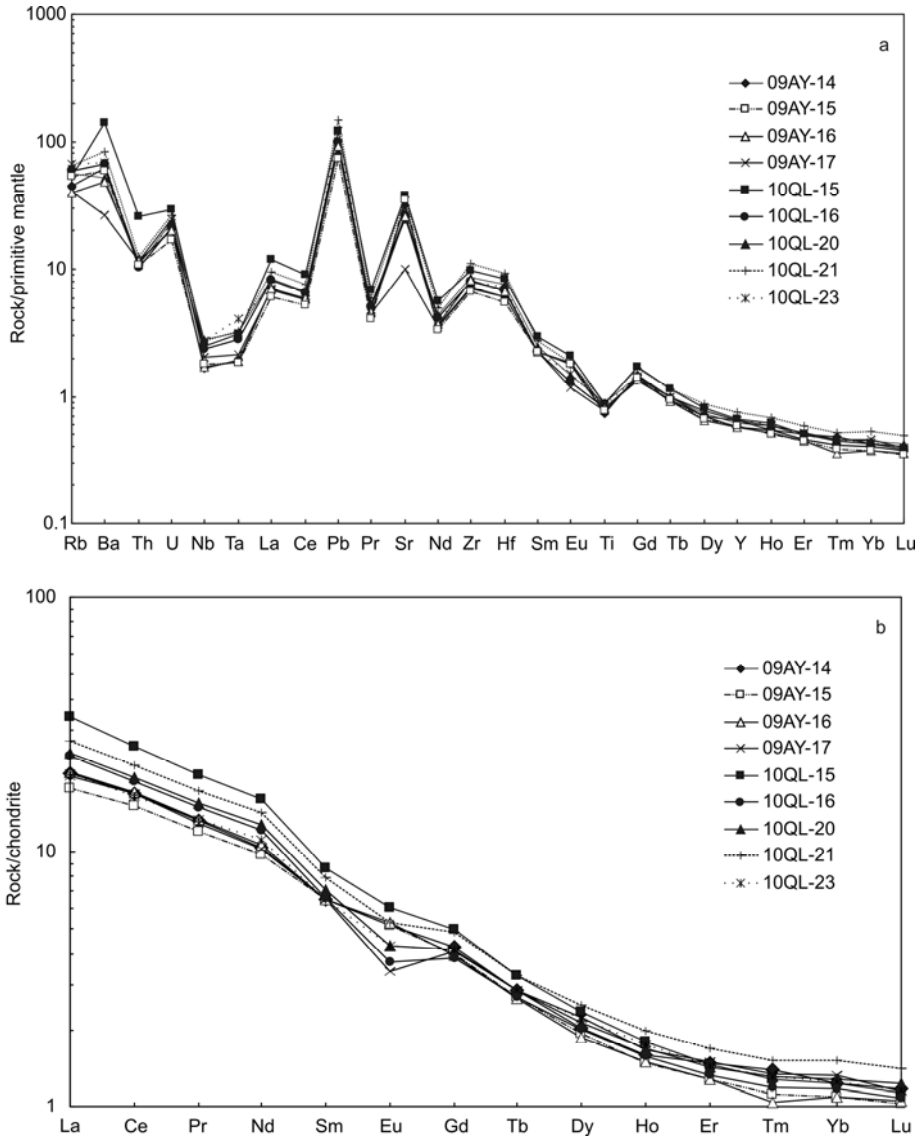

Figure 7 Primitive mantle normalized multi-element (a) and chondrite normalized REE pattern (b) diagrams (standard data from [47]).

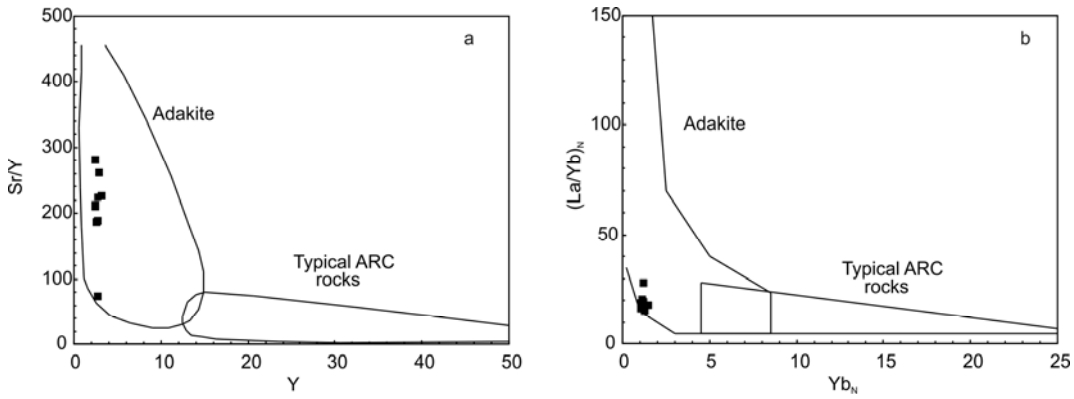

Figure 8 (Sr/Y) vs. Y (a) and $(La/Yb)_N$ vs Yb_N (b) diagrams discriminating between adakite and typical arc calc-alkaline rocks.

Nd isotopic features as those recorded in our samples. Generally, island-arc basalts (IAB) have enriched LILE and LREE which are opposite to mid-ocean ridge basalts (MORB). On the other hand, back-arc basin basalts (BABB) have geochemical characteristics of both IAB and MORB [61–63], with variations depending on extents and positions of partial

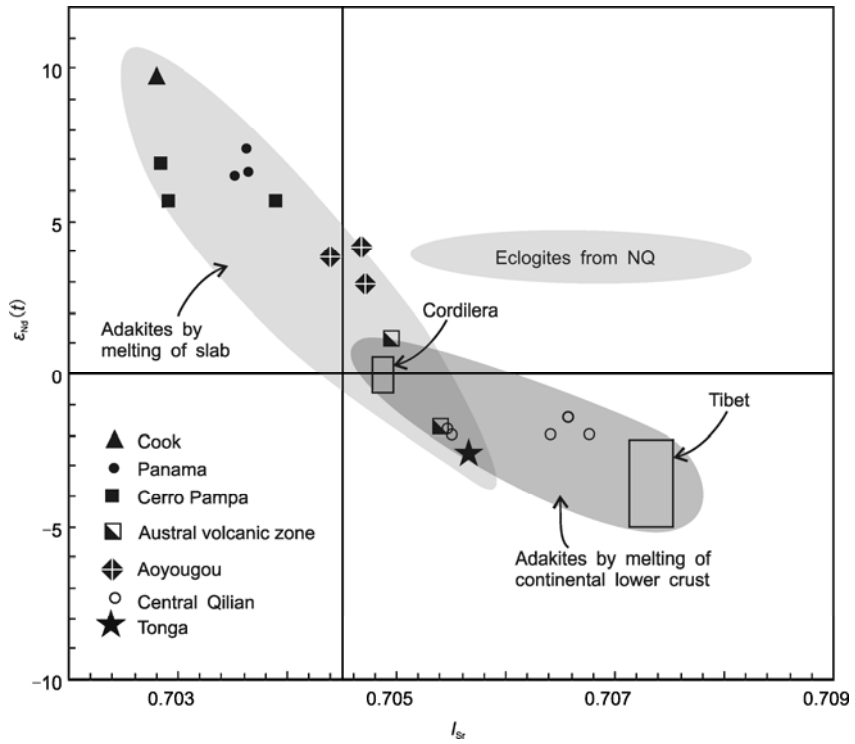

Figure 9 I_{Sr} vs. ε_{Nd} (t=438 Ma) diagram of Aoyougou adakitic rocks comparing with those derived from subducted oceanic slab [4,14,58,64], continental lower crust [25,65,66] and eclogites from the North Qaidam [59].

melting. Since enrichment of LILE and LREE is relatively weak in our samples [$(La)_N$=18–34] (Figure 7b), similar to E-MORB, we prefer that the Aoyougou adakite would be derived from partial melting of the low-K BABB on the oceanic crust. The melting from such oceanic crust would produce granite with felsic, relatively depleted Sr-Nd isotopes and E-MORB-like trace element compositions. Consequently, it is reasonable to conclude that partial melting of the subducted slab can account for the generation of Aoyougou trondhjemites.

5.1 Heat source

In general, slab melting under high pressure lies on a sufficient heat source at special subduction environments, such as high geothermal gradient, hot and young oceanic crust, fast/flat subduction and slab window, where dehydration melting of hydrated minerals would occur [1,6,26]. It should be noted that island-arc volcanic complex and high-pressure metamorphic rocks including lawsonite-bearing blueschist and eclogite are well-developed in the middle part of North Qilian Orogen [33,48,49,51,67], but absent in the studied area. Low subdution angle would be responsible for this absence, similar to the case in the southern island arc of Japan [68,69].

The classic model for slab melting suggests that the subducted oceanic crust would suffer a series of dehydrated reactions during subduction, evolving from greenschist, through amphibolite to eclogite. If the slab becomes hot enough, partial melting in the stability field of garnet generates adakitic melts rather than other felsic melts. In this regard, heating is one of the most important conditions for slab melting. On the other hand, decompression dehydration would also bring about partial melting of HP to UHP metamorphic rocks during their exhumation [70]. Hydrous minerals can break down during decompression exhumation, leading to local sinking of aqueous fluids for partial melting. This has been manifested by studies of field-based petrology and P-T modeling for metamorphic rocks [28–31]. Nahodilova et al. [32] demonstrated that up to 26% of melt lost during transition from early eclogite to granulite-facies conditions thanks to decompression, which is recorded in leucocratic banding in felsic granulites from the Kutna Hora complex in the Moldanubian zone of central Europe. Zhao et al. [71] demonstrated that Late Triassic granites in the Sulu orogen result from decompression melting of the subducted continental crust during exhumation. With respect to the Aoyougou adakite in the North Qilian orogen, its formation age is 20–50 Ma younger than that of eclogite. Thus, it is possible that the adakite would most probably form by decompression melting of the eclogite during exhumation rather than during subduction.

5.2 Pressure

All adakites are characterized by enriched LILE, Pb, LREE, depleted Nb, Ta, Ti, HREE and high Sr/Y ratio (>40). The elevated Sr/Y ratio and depleted HREE in our samples are

commonly interpreted as generating in the depth where garnet is stable. With the development of experimental petrology, rutile is regarded as another necessary residual phase for adakitic magma. However, Foley et al. [72] denied it by consideration that the residue of rutile will affect melt with an elevated Nb/Ta proportion because of $D_{Ta}>D_{Nb}$ between rutile and melt. However, subsequent experiments terrified that hardly can rutile raise the Nb/Tb value of melt, and the residual rutile can account for Nb and Ta negative anomalies in adakite perfectly [21,73–75], which is also observed in our samples. Taking all these features into account, the minimum pressure of 1.5 GPa is required for our samples because breakdown of rutile will happen under the pressure less than 1.5 GPa [21,75]. Geochemical modeling by Moyen [76] revealed that only when garnet emerges ($P>$ 1.5 GPa) can the Sr/Y ratio of the derivative melt be 10 times bigger than that of the parental magma. As the Sr/Y value of oceanic crust generally scatters from 2 to 10, we simply constrain that the minimum pressure of 1.8 GPa (60 km) is demanded for such high Sr/Y ratios of our samples (average 222.5 except for sample 09AY-17) [76].

5.3 Interaction with the mantle wedge

It is commonly though that melts derived from the subducted slab cannot avoid interacting with the mantle wedge through which as it ascends, thus causing higher MgO, Ni and Cr concentrations in adakite when comparing with the experimental melt [57,77]. However, our samples exhibit extremely low MgO, Ni and Cr contents, similar to Archaean TTG (Figure 4g–h), predicting no or limited interaction between adakitic melts and the mantle wedge. Some researchers attributed these features to shallow subduction [7,11,14]. Other two interpretations are also possible. Firstly, following the concept (a=effective melt/mantle peridotite) established by Rapp et al. [77], if the volume of slab melting is large enough, melt created in the early stage will contain less SiO_2, more MgO, Ni and Cr (LSA) than the later HSA because the later melt may go up along the early open path which hinders reactions between the HSA melt and the mantle peridotite. Secondly, if decompression melting of eclogite moves up during exhumation along the subduction channel, it will not pass through mantle wedge and the possibility of melt assimilation by mantle wedge will be zero.

6 Conclusion

Geochemistry demonstrates that the Aoyougou trondhjemite is a high-silica adakite with enriched Na_2O, Sr, Sr/Y, $(La/Yb)_N$, and low K_2O, MgO, Ni and Cr contents, resembling Archean trondhjemite. The initial Sr ratio of 0.7044–0.7047 and $\varepsilon_{Nd}(t)$ of 3.0–4.1 reveal that these rocks are derived from the juvenile ocean crust.

SHRIMP U-Pb dating of zircons gives a concordant age of 438±3 Ma, later than the formation of island-arc volcanic rocks and high-pressure metamorphic rocks in the North Qilian suture zone, suggesting that Aoyougou granite may link to the exhumation of high-pressure metamorphic rocks.

The plausible model for the Aoyougou adakite is that the subducted slab transformed into eclogite in 460–490 Ma, and started to melt by decompressin at the depth of ~60 km at ~438 Ma during exhumation.

We thank D. Y. Liu, H. Q. Jie and L. Su for their help with the lab work, H. Martin for providing the HSA and LSA data. We also thank two anonymous reviewers and Editor Y. F. Zheng for their constructive review comments, which led to a better presentation of the final product. This work was supported by the National Basic Research Program of China (2009CB825007), the National Natural Science Foundation of China (40825007 and 40821002) and the Chinese Geological Survey Projects (1212011121258).

1 Defant M J, Drummond M S. Derivation of some modern arc magmas by melting of young subducted lithosphere. Nature, 1990, 347: 662–665
2 Kay R W. Aleutian magnesian andesites: Melts from subducted Pacific ocean crust. J Volcanol Geoth Res, 1978, 4: 117–132
3 Defant M J, Clark L F, Stewart R H, et al. Andesite and dacite genesis via contrasting processes: The geology and geochemistry of E1 Valle Volcano, Panama. Contrib Mineral Petrol, 1991, 106: 309–324
4 Defant M J, Jackson T E, Drummond M S, et al. The geochemistry of young volcanism throughout western Panama and southeastern Costa Rica: an overview. J Geol Soc Lond, 1992, 149: 569–579
5 Yogodzinski G M, Kelemen P B. Slab melting in Aleutians: Implications of an ion probe study of clinopyroxene in primitive adakite and basalt. Earth Planet Sci Lett, 1998, 158: 53–65
6 Yogodzinski G M, Lees J M, Churikova T G, et al. Geochemical evidence for the melting of subducting oceanic lithosphere at plate edges. Nature, 2001, 409: 500–504
7 Martin H. Adakitic magmas: Modern analogues of Archaean granitoids. Lithos, 1999, 46: 411–429
8 Martin H, Smithies R H, Rapp R, et al. An overview of adakite, tonalite-trondhjemite-granodiorite (TTG), and sanukitoid: Relationships and some implications for crustal evolution. Lithos, 2005, 79: 1–24
9 Smithies R H. The Archaean tonalite-trondhjemite-granodiorite (TTG) series is not an analogue of Cenozoic adakite. Earth Planet Sci Lett, 2000, 182: 115–125
10 Condie K C. TTGs and adakites: Are they both slab melts? Lithos, 2005, 80: 33–44
11 Naqvi S M, Rana Prathap J G. Geochemistry of adakites from Neoarchaean active continental margin of Shimoga schist belt, Western Dharwar Craton, India: Implications for the genesis of TTG. Precambrian Res, 2007, 156: 32–54
12 Naqvi S M, Mohan M R, Rana Prathap J G, et al. Adakite-TTG connection and fate of Mesoarchaean basaltic crust of Holenarsipur Nucleus, Dharwar Craton, India. J Asian Earth Sci, 2009, 35: 416–434
13 Sajona F G, Maury R C, Bellon H, et al. Initiation of subduction and the generation of slab melts in western and eastern Mindanao, Philippines. Geology, 1993, 21: 1007–1010
14 Falloon T J, Danyushevsky L V, Crawford A J, et al. Boninites and adakites from the northern termination of the Tonga trench: Implications for adakite petrogenesis. J Petrol, 2008, 49: 697–715
15 Hou Z Q, Gao Y F, Qu Z Y, et al. Origin of adakitic intrusives generated during mid-Miocene east-west extension in southern Tibet. Earth Planet Sci Lett, 2004, 220: 139–155
16 Chung S L, Liu D Y, Ji J Q, et al. Adakites from continental collision zones: Melting of thickened lower crust beneath southern Tibet. Geology, 2003, 31: 1021–1024

17 Gao S, Rudnick R L, Yuan H L, et al. Recycling lower continental crust in the North China Craton. Nature, 2004, 432: 892–897
18 Xu W L, Wang Q H, Wang D Y, et al. Mesozoic adakitic rocks from the Xuzhou-Suzhou area, eastern China: Evidence for partial melting of delaminated lower continental crust. J Asian Earth Sci, 2006, 27: 454–464
19 Zhang Q, Wang Y, Qian Q, et al. The characterisitics and tectonic metallogenic significances of the adakites in Yanshan period from eastern China (in Chinese). Acta Petrol Sin, 2001, 17: 236–244
20 Zhang Q, Xu J F, Wang Y, et al. Diversity of adakite (in Chinese). Geol Bull Chin, 2004, 23: 959–965
21 Zhang Q, Wang Y, Xiong X L, et al. Adakite and Granite: Challenge and Opportunity (in Chinese). Beijing: China Land Press, 2008. 19–68
22 Macpherson C G, Dreher S T, Thirwall M F. Adakites without slab melting: high pressure processing of island arc Magma, Mindanao, the Philippines. Earth Planet Sci Lett, 2006, 243: 581–593
23 Castillo P R. An overview of adakite petrogenesis. Chin Sci Bull, 2006, 51: 257–268
24 Castillo P R, Janney P E, Solidum R U. Petrology and geochemistry of Camiguin Island, southern Philippines: Insights to the source of adakites and other lavas in a complex arc setting. Contrib Mineral Petrol, 1999, 134: 33–51
25 Tseng C Y, Yang H J, Yang H Y, et al. Continuity of the North Qilian and North Qinling orogenic belts, Central Orogenic System of China: Evidence from newly discovered Paleozoic adakitic rocks. Gondwana Res, 2009, 16: 285–293
26 Gutscher M-A, Maury R, Eissen J-P, et al. Can slab melting be caused by flat subduction? Geology, 2000, 28: 535–538
27 Winter J D. An Introduction to Igneous and Metamorphic Petrology. 2nd ed. New York: Prentice Hall, 2010
28 Sisson T W, Bronto S. Evidence for pressure-release melting beneath magmatic arcs from basalt at Galunggung, Indonesia. Nature, 1998, 391: 883–886
29 Carson C J, Powell R, Wilson C J L, et al. Partial melting during tectonic exhumation of a granulite terrane: An example from the Larsemann Hills, East Antarctica. J Metamorph Geol, 1997, 15: 105–126
30 Bhattacharya S. Archean high-T decompression and partial melting in the Eastern Ghats Belt, India: Correlation with the Antarctic Napier Complex. Gondwana Res, 2001, 4: 575–576
31 Norlander B H, Whitney D L, Teyssier C, et al. Partial melting and decompression of the Thor-Odin dome, Shuswap metamorphic core complex, Canadian Cordillera. Lithos, 2002, 61: 103–125
32 Nahodilova R, Faryad S W, Dolejs D, et al. High-pressure partial melting and melt loss in felsic granulites in the Kutna Hora complex, Bohemian Massif (Czech Republic). Lithos, 2011, 125: 641–658
33 Song, S G, Zhang L F, Niu Y L, et al. Evolution from oceanic subduction to continental collision: A case study of the Northern Tibetan Plateau inferred from geochemical and geochronological data. J Petrol, 2006, 47: 435–455
34 Feng Y M, He S P. Geotectonics and Orogeny of the Qilian Mountain (in Chinese). Beijing: Geological Publishing House, 1996. 1–135
35 Song S G, Niu Y L, Zhang L F, et al. Tectonic evolution of Early Paleozoic HP metamorphic rocks in the North Qilian Mountains, NW China: New perspectives. J Asian Earth Sci, 2009, 35: 334–353
36 Xiao X C, Chen G M, Zhu Z Z. A preliminary study on the tectonics of ancient ophiolites in the Qilian Mountains, northwest China (in Chinese). Acta Geol Sin, 1978, 52: 287–295
37 Xiang Z Q, Lu S N, Li H K, et al. SHRIMP U-Pb zircon age of gabbro in Aoyougou in the western segment of the North Qilian Mountain, China and its geological implications (in Chinese). Geol Bull Chin, 2007, 26: 1686–1691
38 Song S G, Niu Y L, Su L, et al. Tectonics of the North Qilian Orogen, NW China. Gondwana Res, 2012, doi: 10.1016/j.gr.2012.02.004
39 Ludwig K R. Users Manual for Isoplot/Ex rev. 2.49. Berkeley Geochronology Centre, 2001, Spec Publ (1): 56
40 Song B, Zhang Y H, Liu D Y. Introduction to the Naissance of SHRIMP and its contribution to isotope geology (in Chinese). J Chin Mass Spect Soc, 2002, 23: 58–62
41 Williams I S. U-Th-Pb geochronology by ion microprobe. Rev Ecol Geol, 1998, 7: 1–35
42 Song S G, Su L, Li X H, et al. Tracing the 850-Ma continental flood basalts from a piece of subducted continental crust in the North Qaidam UHPM belt, NW China. Precambrian Res, 2010, 183: 805–816
43 Jahn B-M, Cornichet J, Cong B, et al. Ultrahigh-ε_{Nd} eclogites from an ultrahigh-pressure metamorphic terrane of China. Chem Geol, 1996, 127: 61–79
44 Barker F, Arth J G. Generation of trondhjemitic–tonlaitic liquids and Archaean bimodal trondhjemite–basalt suites. Geology, 1976, 4: 596–600
45 Martin H. The Archaean grey gneisses and the genesis of the Continental Crust. In: Condie K C, ed. The Archaean Crustal Evolution. Amsterdam: Elsevier, 1995. 205–259
46 Li X H, Li Z X, Ge W C, et al. Neoproterozoic granitoids in South China: Crustal melting above a mantle plume at ca. 825 Ma? Precambrian Res, 2003, 122: 45–83
47 Sun S S, McDonough W F. Chemical and isotopic systematics of oceanic basalt: Implications for Mantle composition and processes. In: Saunders A D, Norry M J, eds. Magmatism in the Ocean Basins. Geol Soc Spec Publ, 1989, 42: 528–548
48 Song S G, Zhang L F, Niu Y L, et al. Zircon U-Pb SHRIMP ages of eclogites from the North Qilian Mountains, NW China and their tectonic implication. Chin Sci Bull, 2004, 49: 848–852
49 Zhang J X, Meng F C, Wan Y S. A cold Early Paleozoic subduction zone in the North Qilian Mountain, NW China: Petrological and U-Pb geochronological constraints. J Metamorph Geol, 2007, 25: 285–304
50 Zhang J X, Xu Z Q, Chen W, et al. A tentative discussion on the ages of the subduction- accretionary complex/volcanic arcs in the middle sector of North Qilian Mountain (in Chinese). Acta Petrol Mineral, 1997, 16: 112–119
51 Wu H Q, Feng Y M, Song S G. Metamorphism and deformation of blueschist belts and their tectonic implications, North Qilian Mountains, China. J Metamorph Geol, 1993, 11: 523–536
52 Liou J G, Wang X M, Colemen R G. Blueschists in major suture zones of China. Tectonics, 1989, 8: 609–619
53 Song S G, Zhang L F, Niu Y, et al. Early Paleozoic plate-tectonic evolution and deep continental subduction on the northern margin of the Qinghai-Tibet Plateau (in Chinese). Geol Bull Chin, 2004, 23: 918–925
54 Wu C L, Xu X Y, Gao Q M, et al. Early Palaezoic granitoid magmatism and tectonic evolution in North Qilian, NW China (in Chinese). Acta Petrol Sin, 2010, 26: 1027–1044
55 Rapp R P, Watson E B, Miller C F. Partial melting of amphibolite, eclogite and the origin of Archaean trondhjemites and tonalities. Precambrian Res, 1991, 51: 1–25
56 Sen C, Dunn T. Dehydration melting of a basaltic composition amphibolites at 1.5 and 2.0 GPa: Implications for the origin of adakites. Contrib Mineral Petrol, 1994, 117: 394–409
57 Prouteau G, Scaillet B, Pichavant M, et al. Evidence for mantle metasomatism by hydrous silicic melts derived from subducted oceanic crust. Nature, 2001, 410: 197–200
58 Futa K, Stern C R. Sr and Nd isotopic and trace element compositions of Quaternary volcanic centers of the southern Andes. Earth Planet Sci Lett, 1988, 88: 253–263
59 Zhang G B, Song S G, Zhang L F, et al. The subducted oceanic crust within continental-type UHP metamorphic belt in the North Qaidam, NW China: Evidence from petrology, geochemistry and geochronology. Lithos, 2008, 104: 99–118
60 Paquette J L, Menot R P, Peucat J J. REE, Sm/Nd and U-Pb zircon study of eclogites from the Alpine External Massifs (Western Alps): Evidence for crustal contamination. Earth Planet Sci Lett, 1989, 96: 181–198
61 Taylor B, Martinez F. Back-arc basin basalt systematics. Earth Planet Sci Lett, 2003, 210: 481–497
62 Pearce J A, Stern R J. The origin of back-arc basin magmas: Trace element and isotope perspectives. In: Back-Arc Spreading Systems: Geological, Biological, Chemical and Physical Interactions. Amer Geophys Union Geophys Monogr, 2006, 166: 63–86
63 Xia X H, Song S G. Forming age and tectono-petrogenises of the Jiugequan ophiolite in the North Qilian Mountain, NW China. Chin

Sci Bull, 2010, 55: 1899–1907
64 Kay S M, Romas V A, Marquez M. Evidence in Cerro Pampa volcanic rocks for slab-melting prior to ridge-trench collision in southern south America. Geology, 1993, 101: 703–714
65 Wang Q, McDermott F, Xu J F, et al. Cenozoic K-rich adakitic volcanic rocks in the Hohxil area, northern Tibet: Low crustal melting in an intracontinental setting. Geology, 2005, 33: 465–468
66 Petford N, Atherton M. Na-rich partial melts from newly underplated basaltic crust: The Cordillera Blanca Batholith, Peru. J Petrol, 1996, 37: 1491–1521
67 Zhang L F, Wang Q J, Song S G. Lawsonite blueschist in Northern Qilian, NW China: P-T pseudosections and petrologic implications. J Asian Earth Sci, 2009, 35: 354–366
68 Morris P A. Slab melting as an explanation of Quaternary volcanism and aseismicity in southwest Japan. Geology, 1995, 5: 395–398
69 Peacok S M, Wang K. Seismic consequences of warm versus cool subduction metamorphism: Examples from southwest and northeast Japan. Science, 1999, 286: 937–939
70 Zheng Y F, Xia Q X, Chen R X, et al. Partial melting, fluid supercriticality and element mobility in ultrahigh-pressure metamorphic rocks during continental collision. Earth Sci Rev, 2011, 107: 342–374
71 Zhao Z F, Zheng Y F, Zhang J, et al. Syn-exhumation magmatism during continental collision: Evidence from alkaline intrusives of Triassic age in the Sulu orogen. Chem. Geology, 2012, doi: 10.1016/j.chemgeo.2011.11.002
72 Foley S, Tiepolo M, Vannucci R. Growth of early continental crust controlled by melting of amphibolite in subduction zones. Nature, 2002, 417: 837–840
73 Rapp R P, Shimizu N, Norman M D. Growth of early continental crust by partial melting of eclogite. Natrue, 2003, 425: 605–609
74 Kelemen P B, Yogodzinski G M, Scholl D W. Along-strike variation in the Aleutian Island Arc: Genesis of high Mg number andesite and implications for continental crust. Inside the Subduction Factory. Amer Geophys Union Geophys Monogr, 2003, 138: 223–276
75 Xiong X L, Adam J, Green T H. Rutile stability and rutile/melt HFSE partitioning during partial melting of hydrous basalt: Implications for TTG genesis. Chem Geol, 2005, 218: 339–359
76 Moyen J F. High Sr/Y and La/Yb ratios: The meaning of the "adakitic signature". Lithos, 2009, 112: 556–574
77 Rapp R P, Shimizu N, Nor Man M D, et al. Reaction between slab-derived melts and peridotite in the mantle wedge: Experimental constraints at 3.8 GPa. Chem Geol, 1999, 160: 335–356